IPEM
Institute of Physics and
Engineering in Medicine

PAPER • OPEN ACCESS

Magnetic separation of iron oxide nanoparticles to improve their application for magnetic particle imaging

View the article online for updates and enhancements.

Physics in Medicine & Biology

IPEM Institute of Physics and Engineering in Medicine

PAPER

Magnetic separation of iron oxide nanoparticles to improve their application for magnetic particle imaging

Soudabeh Arsalani[1,2] , Norbert Löwa[1], Olaf Kosch[1], Patricia Radon[1], Oswaldo Baffa[2] and Frank Wiekhorst[1]

1   Physikalisch-Technische Bundesanstalt, Abbestrasse 2-12, D-10587 Berlin, Germany
2   Departament of Physics, FFCLRP, University of São Paulo, Av. Bandeirantes 3900, Ribeirão Preto, SP 14040-91, Brazil

E-mail: sarsalani@usb.br

Abstract

Magnetic particle imaging (MPI) is a promising medical imaging technique for visualizing the three-dimensional distribution of tracer materials, specifically iron oxide nanoparticles (IONP). The optimization of magnetic nanoparticles (MNP) plays an essential role to improve the image resolution and sensitivity of imaging techniques. *Objective.* In this work, the optimization of commercial IONP (EMG 700, Ferrotec) coated with anionic surfactants was carried out using magnetic separation (MS) technique, by a low gradient magnetic separation (LGMS) ($<15\,\mathrm{T\,m^{-1}}$) method, to improve their performance as MPI tracers. *Approach.* The magnetophoretical behavior of the samples in different concentrations ranging from 2 to 120 mmol l^{-1} was investigated over 24 h of separation. The samples were characterized by dynamic light scattering (DLS), AC susceptibility (ACS), magnetic particle spectroscopy (MPS) and they were imaged in a preclinical MPI scanner, before and after MS. *Main results.* DLS results showed that by increasing the concentration from 2 to 120 mmol l^{-1} the hydrodynamic diameter of MNP decrease from 75 to 47 nm and size distribution decrease from 0.19 to 0.11 after 4 min MS. In addition, the MPS results demonstrated the third harmonic amplitude normalized to the iron amount (A_3^{*}) and harmonic ratio (A_5/A_3) of signal increase from 8.38 to 10.59 Am^2 kg^{-1} (Fe) and 24.21–26.60, respectively. Furthermore, the MPI images of the samples after separation showed higher MPI resolution. *Significance.* Therefore, LGMS can be considered as a valuable method to narrow and control the size distribution of MNP for MPI.

1. Introduction

Over the last decades, medical imaging technologies such as computed tomography, ultrasound imaging, magnetic resonance imaging (MRI), and positron emission tomography have been playing important roles in clinical diagnosis (Arsalani *et al* 2019b, Umar and Atabo 2019). Compared to these traditional techniques, magnetic particle imaging (MPI) is a rather young 3D imaging modality with high spatial and high temporal resolution which allows tracking and quantification of magnetic nanoparticle (MNP) tracers such as iron oxide nanoparticles (IONP) (Du *et al* 2013, Wu *et al* 2019). IONP are the most frequently used MNP systems employed in biomedical applications due to their high stability, high biocompatibility and magnetization, and low toxicity (Arsalani *et al* 2018, 2019a, Araujo *et al* 2020).

The spatial resolution and sensitivity of the MPI images depend on the applied magnetic field and the properties of the MNP tracers such as the core size, core size distribution, anisotropy of the magnetic core, and surface modification of MNP (Du *et al* 2013, Ziemian *et al* 2018). Numerical simulations of Yoshida *et al* (2017) showed that MPI image quality can efficiently be improved by employing MNP with narrow size distribution and small anisotropy energy. In general, size distribution plays an essential role in biomedical applications, especially *in vivo*, and it is extremely important for evaluation of magnetic properties of MNP (Pacakova *et al* 2017).

Theoretically, particles with a broader size distribution tend to present a higher aggregation rate rather than those with the same size (Petosa *et al* 2010, Mohammed *et al* 2017). Therefore, the large size distribution of MNP can lead to aggregation, resulting in some drawbacks such as changing the magnetic properties of MNP or medical issues (blood clotting, blocking blood vessels and circulation time) (Arami *et al* 2015, Gutiérrez *et al* 2019, Arsalani *et al* 2020). Therefore, some techniques are required and applied to reduce the size distribution. So far, several methods have been reported for MNP such as magnetic field flow fractionation filtration (Latham *et al* 2005, Löwa *et al* 2015b), separation in electric fields (Stephens *et al* 2012), centrifugation (Dadfar *et al* 2020) and gradient magnetic separation (MS) (Löwa *et al* 2015a).

Recently, MS technique, which commonly is classified into low gradient magnetic separation (LGMS) (<100 T m^{-1}) and high gradient magnetic separation (>100 T m^{-1}) (De Las Cuevas *et al* 2008, Yeap *et al* 2017), has gained a great attention in biotechnology applications ranging from wastewater treatments to biomedical applications (Yavuz *et al* 2006, He *et al* 2014, Leong *et al* 2016). The motion of MNP in an inhomogeneous magnetic field is known as magnetophoresis and is characterized by the separation time parameter which is determined by the magnetophoretical velocities of the MNP. Generally, magnetophoresis processes are caused by two principal different types: cooperative magnetophoresis which is a quick process enhanced by interactions of particles, and noncooperative magnetophoresis which is a slow process caused by the movement of the individual particles in magnetic fields (Andreu *et al* 2011, Leong *et al* 2020).

The magnetophoresis process depends on several parameters such as size, size distribution, zeta potential, shape, magnetic moment, concentration of MNP and magnetic field gradient (Benelmekki *et al* 2011, Leong *et al* 2016, Leong *et al* 2017). Some researchers have been investigating the effect of these parameters on separation time of MNP by magnetophoresis experiments. For instance, Lim *et al* studied the effect of MNP shape on separation time, showing that the separation time of nanorods is shorter than of nanospheres (Lim *et al* 2014). The effect of zeta potential on magnetophoretical behavior was investigated by Benelmekki *et al* (2011). They found increased separation times for MNP with higher zeta potential. Furthermore, De Las Cuevas *et al* (2008) investigated the effect of concentration on separation time for MNP over a few minutes of MS in a homogeneous 30 T m^{-1} gradient.

Mostly, inhomogeneous gradients are used in MS techniques. However, in an inhomogeneous magnetic field gradient, the magnetic force on the MNP is different at every point of the system that can lead to an uncontrolled and unrepeatable separation process. The significant advantage of using a homogeneous gradient is that the MNP experience identical magnetic forces everywhere in the system and the separation process is performed under more precisely controlled homogeneous conditions. Therefore, changes in the separation processes can more directly be related to characteristics of MNP and/or sample viscosity. In the present study, we treated the commercial IONP (EMG 700) with MS technique using a homogeneous magnetic field gradient of 15 T m^{-1}, to improve their capability for biomedical applications such as MPI tracer. In addition, we investigated the magnetophoretical behavior of IONP at different concentrations in the range 2–120 mmol l^{-1} over a 24 h time period. We demonstrate that LGMS is a quick and efficient technique to narrow the size distribution of MNP in aqueous phase and to improve their magnetic properties for biomedical applications such as MPI.

2. Materials and methods

2.1. Materials
In this work, commercial IONP (EMG 700, FerroTec) with 10 nm core size and zeta potential of -34 mV were used. These MNP have a magnetite core (Fe$_3$O$_4$) with an anionic surfactant coating. They are currently employed in basic physics and biomedical research. A blue and black liquid ink were used as a control to study the optical dynamic range of the detector of the magnetophoretic system. In this study, the samples were named 'EM' followed by their concentration value, for example an EM sample with 8 mmol l^{-1} concentration was denoted as 'EM8'.

2.2. Magnetophoresis experiment
The magnetophoretical behavior of MNP in aqueous phase was studied by a magnetophoresis device (Sepmag Systems, SL, Barcelona, Spain). This device provides a homogeneous magnetic field gradient and contains of three cylindrical cavities, two of them for 2 ml volume tubes and one for a 15 ml tube. This device is designed to provide a uniform magnetic gradient of 15 T m^{-1} to supply uniform magnetophoretic conditions in the cylindrical cavities. The magnetic force experienced by the magnetic particles is given by (Benelmekki *et al* 2012):
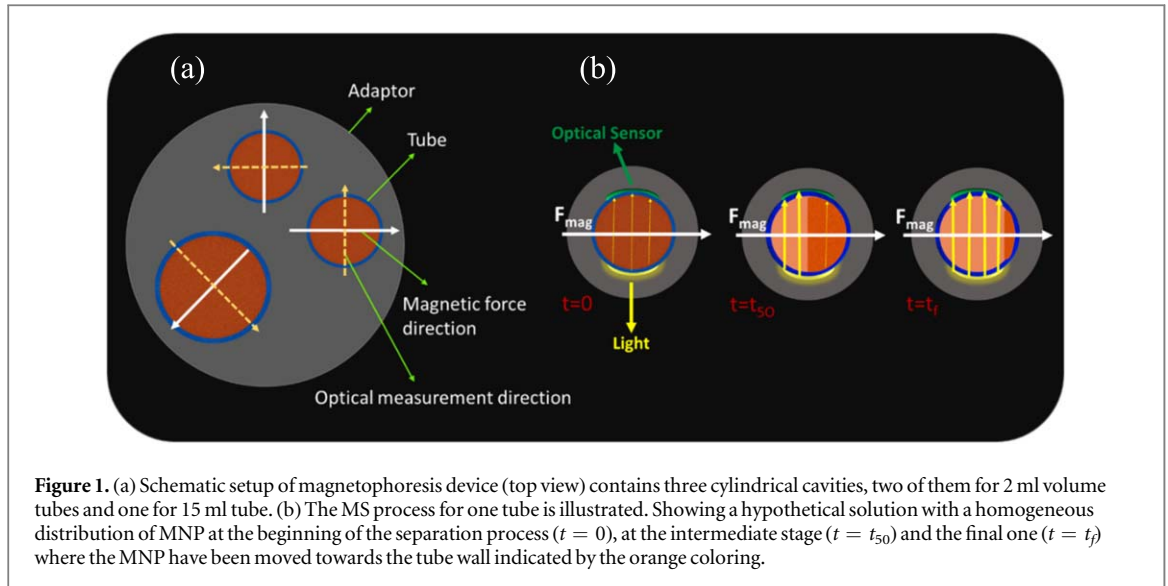
Figure 1. (a) Schematic setup of magnetophoresis device (top view) contains three cylindrical cavities, two of them for 2 ml volume tubes and one for 15 ml tube. (b) The MS process for one tube is illustrated. Showing a hypothetical solution with a homogeneous distribution of MNP at the beginning of the separation process ($t = 0$), at the intermediate stage ($t = t_{50}$) and the final one ($t = t_f$) where the MNP have been moved towards the tube wall indicated by the orange coloring.

$$F_m = m\mu_0 \frac{\partial H}{\partial r}, \tag{1}$$

where m is the magnetic moment of the nanoparticle, μ_0 is the magnetic constant, and $\frac{\partial H}{\partial r}$ is the radial magnetic gradient. The magnetic force causes the particles to move with a magnetophoretical velocity. The velocity of the magnetic particles depends on the balance between the applied magnetic force and the drag force. The magnitude of drag force can be evaluated by (Lim *et al* 2011):

$$F_d = 3\pi\eta \mathrm{dh}v. \tag{2}$$

Here, η is the viscosity of the carrier fluid, dh the hydrodynamic diameter and v the particle velocity.

The schematic setup and process of the magnetophoresis technique are depicted in figures 1(a), (b), respectively. In this setup the optical measurement direction is perpendicular to the magnetic force direction (figure 1(a)). The MNP in the sample volume move towards the wall of the sample tube with a certain velocity, changing the transparency of the detection area of the light sensor over time (figure 1(b)). The half separation time (t_{50}) and slope (defined by the dimensionless exponent 'p') of magnetophoresis curves were calculated by fitting a logistic function ($y = A_2 + \frac{(A_1 - A_2)}{(1 + x/x_0)^p}$) to the measurement data.

2.3. Dynamic light scattering (DLS)
The hydrodynamic diameter (d_h) and polydispersity index (PDI) of samples were determined by DLS using a Zetasizer system (Malvern Instruments, UK) to study the magnetophoresis behavior of samples and the effect of concentration on the separation of agglomerated MNP in suspension during the MS process. About 200 μl sample volume were taken from the center of the Eppendorf cup at different time points during the separation procedure. This device is equipped with a He/Ne laser with a wavelength of 632.8 nm illuminating the sample. The scattered light is detected at a scattering angle of 173°. All measurements were performed at $T = 20$ °C. The d_h values are reported as intensity weighted average diameters.

2.4. AC susceptibility (ACS)
To determine the particle cluster sizes and the agglomeration of MNP, ACS measurements were performed using a Dynomag system (Rise Acreo, Sweden) (Ahrentorp *et al* 2017). In this method, the real part (in-phase component) χ' and imaginary part (out-of-phase component) χ'' of the linear magnetic susceptibility are measured at excitation frequencies in the range 1 Hz–500 kHz. All measurements were performed at 25 °C on MNP suspensions with a volume of 100 μl. By fitting the experimental data to a Debye model (multi-core model), which has been written in detail in reference (Ludwig *et al* 2017), d_h and size distribution (σ) of MNP clusters were determined.

2.5. Magnetic particle spectroscopy (MPS)
To investigate the magnetic properties of the samples the dynamic nonlinear magnetic susceptibility of samples, before and after MS, was measured by a MPS device (MPS-3, Bruker Biospin, Germany) (Biederer *et al* 2009). Furthermore, since MPS is based on the same physical principle as MPI, therefore it is a suitable technique for tracer evaluation (Löwa *et al* 2015a). MPS device consists of a drive field coil and a receiving pick-up coil
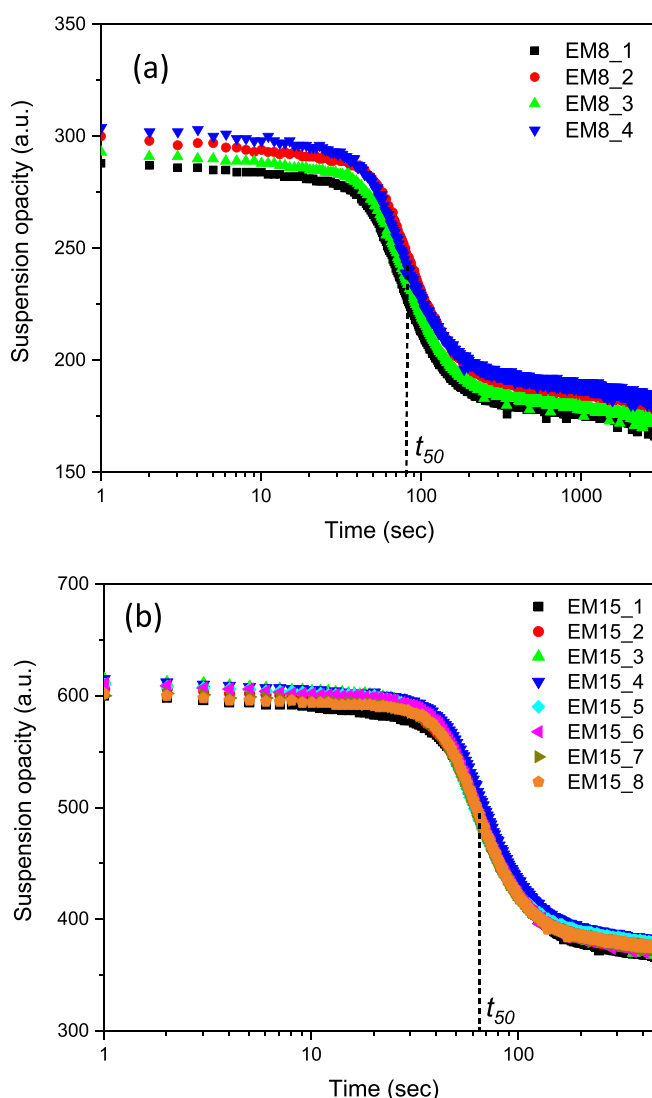
Figure 2. (a) Reproducibility of LGMS: four different samples of 8 mmol l^{-1} concentration (EM8), and (b) the subsequent repetitions of the magnetophoresis experiments for one identical sample with 15 mmol l^{-1} concentration (EM15).

surrounded by an electromagnetic shielding. For measurements, we used a 30 μl sample volume filled into a PCR tube placed in the pick-up coil system of the device. The nonlinear magnetic response of MNP was recorded at a drive field amplitude of 25 mT and (fixed) excitation frequency ($f_{\text{excite}} = 25$ kHz) at 37 °C. After filtering to suppress the excitation signal and Fourier transform the MPS spectrum of MNP shows amplitudes at odd multiples of the excitation frequency (A_i with $i = 3, 5, 7$, etc). We used the third harmonic amplitude normalized to the iron amount (A_3^*) and the harmonic ratio A_5/A_3 as an indicator for the slope of the spectrum.

2.6. Magnetic particle imaging

MPI measurements were performed using a preclinical 3D-MPI system (Bruker BioSpin GmbH, Ettlingen, Germany) working at three slightly different drive field frequencies of about 25 kHz for the three orthogonal dimensions (x, y, z) using amplitudes of 12 mT and a selection gradient of 2.5 T m^{-1} in z-direction and 1.25 T m^{-1} in x- and y-directions. Image reconstructions were performed based on the system function (SF) approach in the frequency domain using a small (point-like) reference sample measured with identical parameters for all MNP systems (25 × 25 × 13 voxels, 100 averages and subtraction of background measured all 25 voxels and a repetition rate of 5). A more detailed description is given in (Rahmer *et al* 2009, 2012). To compare MPI resolution for samples before and after MS, we applied 200 μl of EM15 and EM120 samples after 4 min of MS in a phantom consisting of a spiral channel with a quadratic cross-section of 2 × 2 mm 20 × 20 × 4 mm^3-plastic carrier (Kosch *et al* 2019). The concentrations of EM15 and EM120 samples after 4 min of separation were determined by phenanthroline spectrophotometric iron quantification assay about 10 and 55 mmol l^{-1}, respectively. Therefore, we diluted EM15 and EM120 samples to the same concentration (10 and 55 mmol l^{-1}), without inserting in the MS system, compared to the samples after MS and applied them in
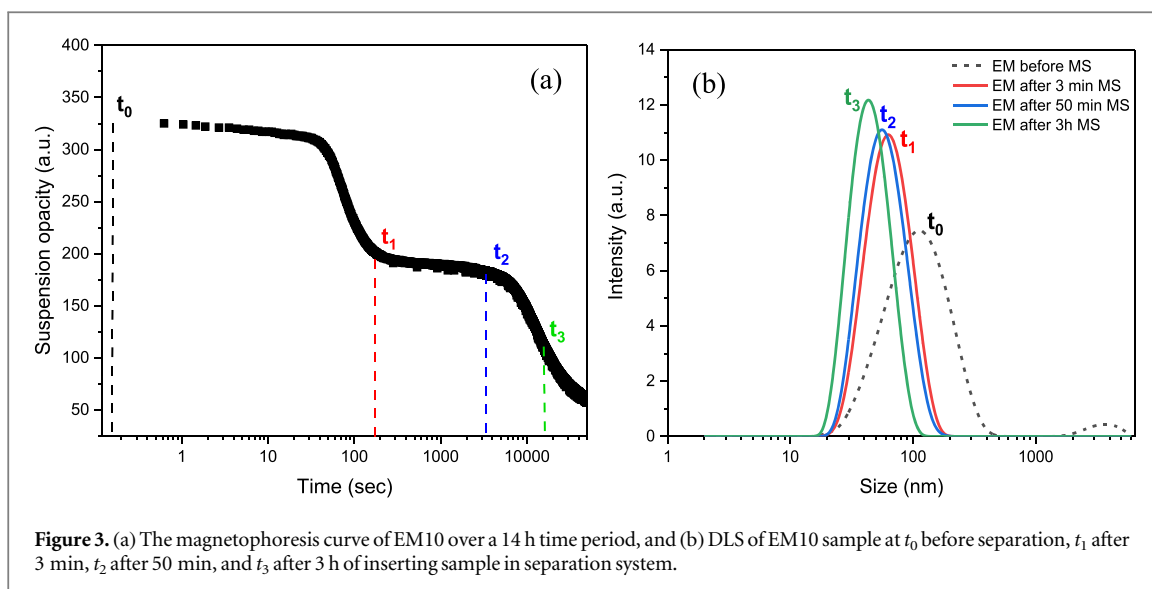
Figure 3. (a) The magnetophoresis curve of EM10 over a 14 h time period, and (b) DLS of EM10 sample at t_0 before separation, t_1 after 3 min, t_2 after 50 min, and t_3 after 3 h of inserting sample in separation system.
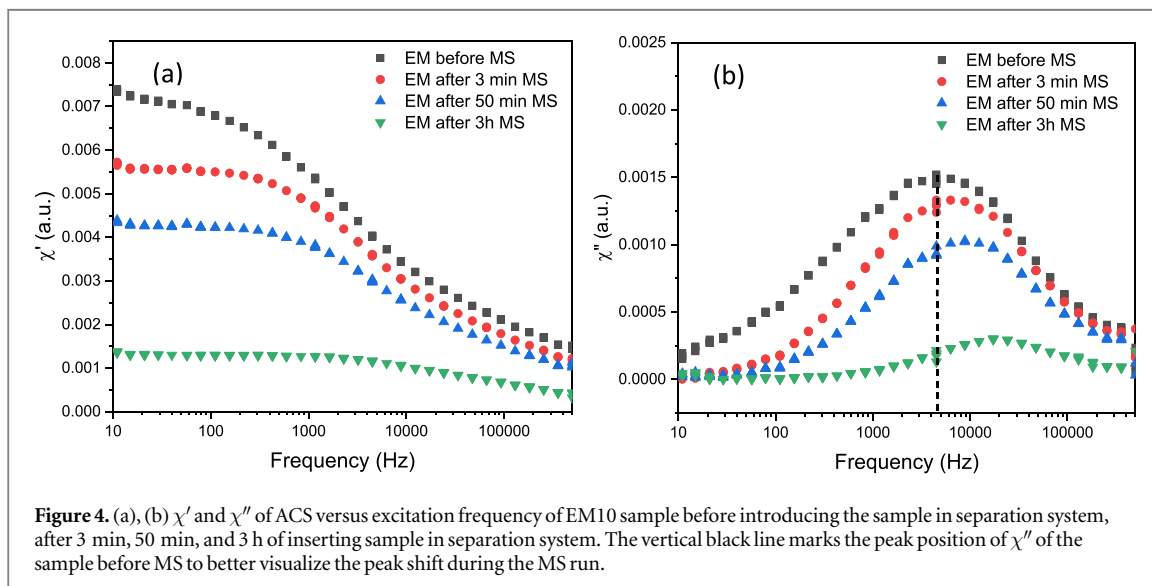
Figure 4. (a), (b) χ' and χ'' of ACS versus excitation frequency of EM10 sample before introducing the sample in separation system, after 3 min, 50 min, and 3 h of inserting sample in separation system. The vertical black line marks the peak position of χ'' of the sample before MS to better visualize the peak shift during the MS run.
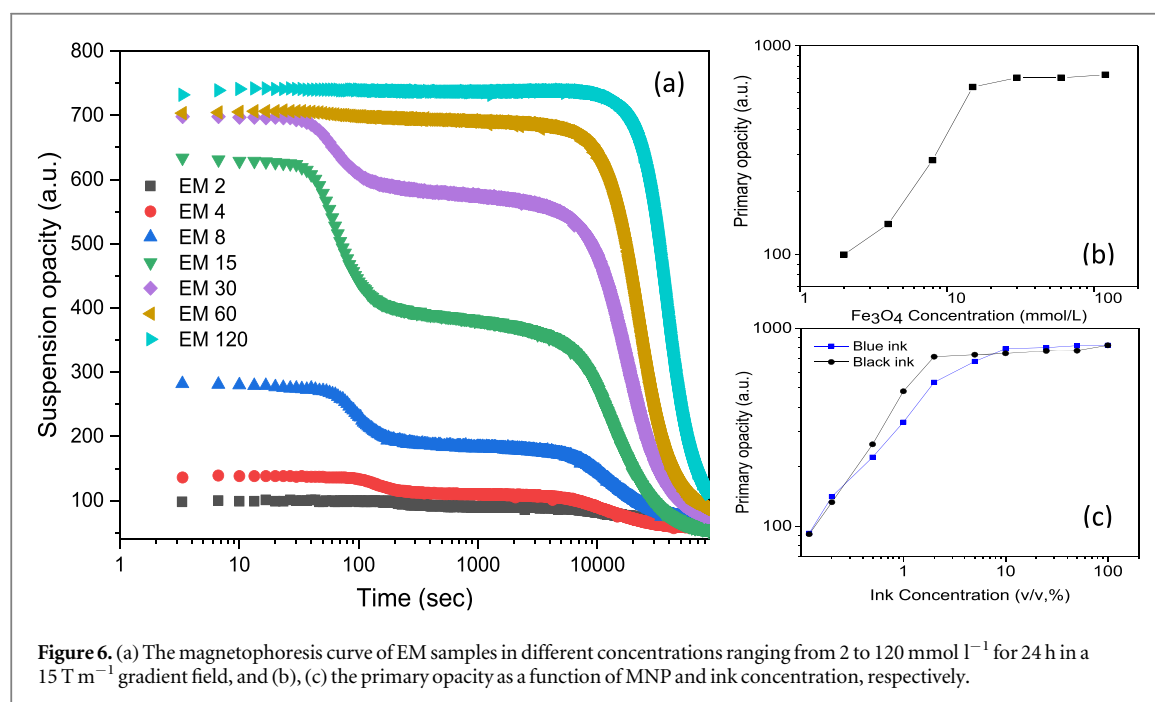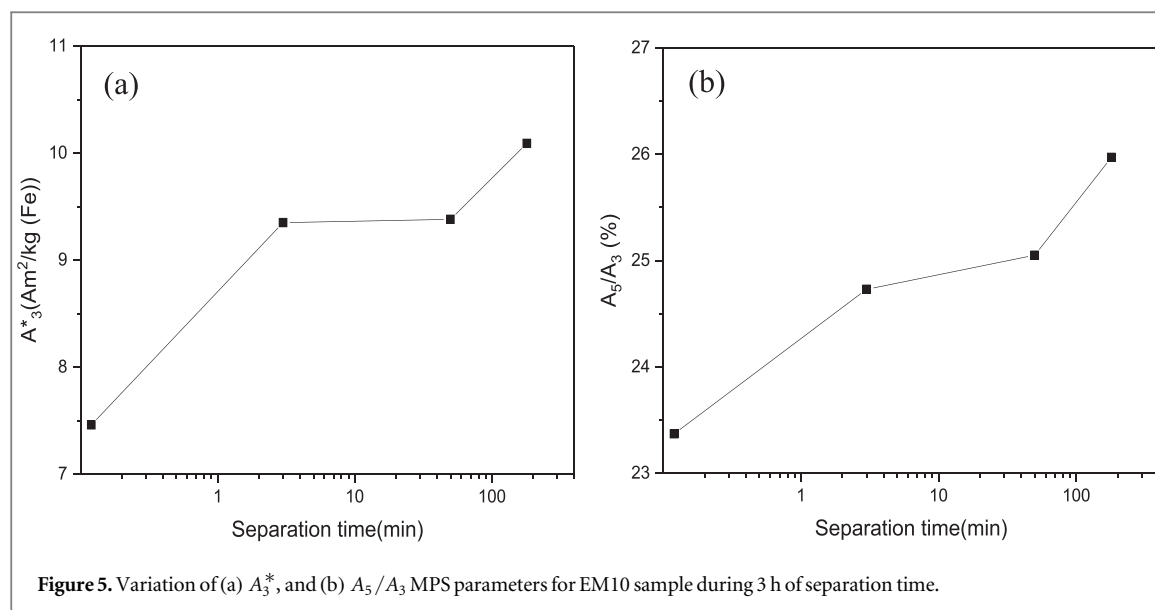
the MPI measurements. Four SFs of the tracer were recorded, before and after the MS and for 10 and 55 mmol l^{-1}. Image reconstructions with a field of view of $25 \times 25 \times 13$ mm^3 and $1 \times 1 \times 1$ mm^3 voxel size was performed using a signal-to-noise-ratio (SNR) $\geqslant 4$, 20 Kaczmarz-iterations, and a regularization parameter $\lambda = 10^{-5}$.

3. Results

The reproducibility of the separation runs was investigated by recording the magnetophoresis curves of four EM samples with the same concentration of 8 mmol l^{-1} (EM8) for 3000 s (figure 2(a)). The mean t_{50} and p of these curves were 81(1.3) s and 3(0.06), respectively. As can be seen, the relative standard deviations of both values of about 2% underline the high reproducibility conditions of the separation system.

Furthermore, the reversibility of magnetophoresis process was studied by recording eight times the magnetophoresis curve of one identical EM sample with a concentration of 15 mmol l^{-1} (EM15) for 500 s. In figure 2(b) the recorded curves of the eight measurements show no significant changes in amplitude and shape. The average t_{50} and p of the curves were 66(2) s and 2.8(0.3), respectively. Therefore, magnetophoresis process can be considered as a reversible process.

The magnetophoretical behavior of a sample with 10 mmol l^{-1} concentration (EM10) was shown in figure 3(a) over a 14 h time period. The magnetophoresis curve of this sample consists of two distinct steps which can be ascribed to the extraction of MNP with different sizes. To clarify this, we determined d_h and PDI by DLS for the EM10 sample material in different time point of separation process. Figure 3(b) shows the DLS curves of

Figure 5. Variation of (a) A_3^*, and (b) A_5/A_3 MPS parameters for EM10 sample during 3 h of separation time.

Figure 6. (a) The magnetophoresis curve of EM samples in different concentrations ranging from 2 to 120 mmol l^{-1} for 24 h in a 15 T m^{-1} gradient field, and (b), (c) the primary opacity as a function of MNP and ink concentration, respectively.

Table 1. The characteristics of the EM10 sample before MS and during 3 h of MS by DLS, ACS and MPS.

Sample EM10	d_h DLS (nm)	PDI DLS	d_h ACS (nm)	σ ACS	A_3^* (Am^2 kg^{-1} (Fe))	A_5/A_3 (%)
Before MS (t_0)	113	0.25	50.0	2.16	7.46	23.37
After 3 min MS (t_1)	62	0.14	40.7	1.79	9.35	24.73
After 50 min MS (t_2)	56	0.13	37.5	1.75	9.38	25.05
After 3 h MS (t_3)	44	0.11	26.5	1.75	10.09	25.97

the EM10 before applying the magnetic field gradient (time point t_0), e.g. before introducing the sample into the separation device, $t_1 = 3$ min shortly after the first step, $t_2 = 50$ min, and $t_3 = 3$ h during the second step.

As it can be seen in table 1 the d_h and PDI significantly changes (about 45%) from t_0 to t_1, while a slight difference is observed in the PDI for time points later than t_1. These results show that the MS removes magnetic entities of different sizes.

The ACS measurements for EM10 sample at different time points during the separation process were shown in figures 4(a), (b). The signal in both χ' and χ'' decrease with increasing separation time up to 3 h. Furthermore,
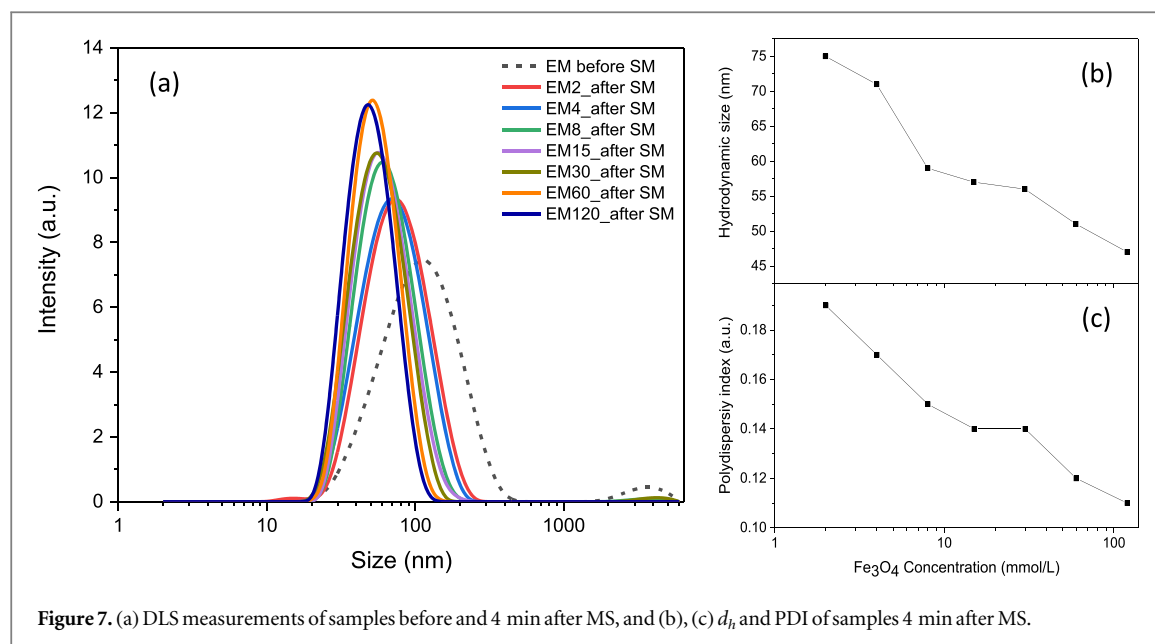
Figure 7. (a) DLS measurements of samples before and 4 min after MS, and (b), (c) d_h and PDI of samples 4 min after MS.

Figure 8. Picture of the phantom filled with 200 μl of tracer.
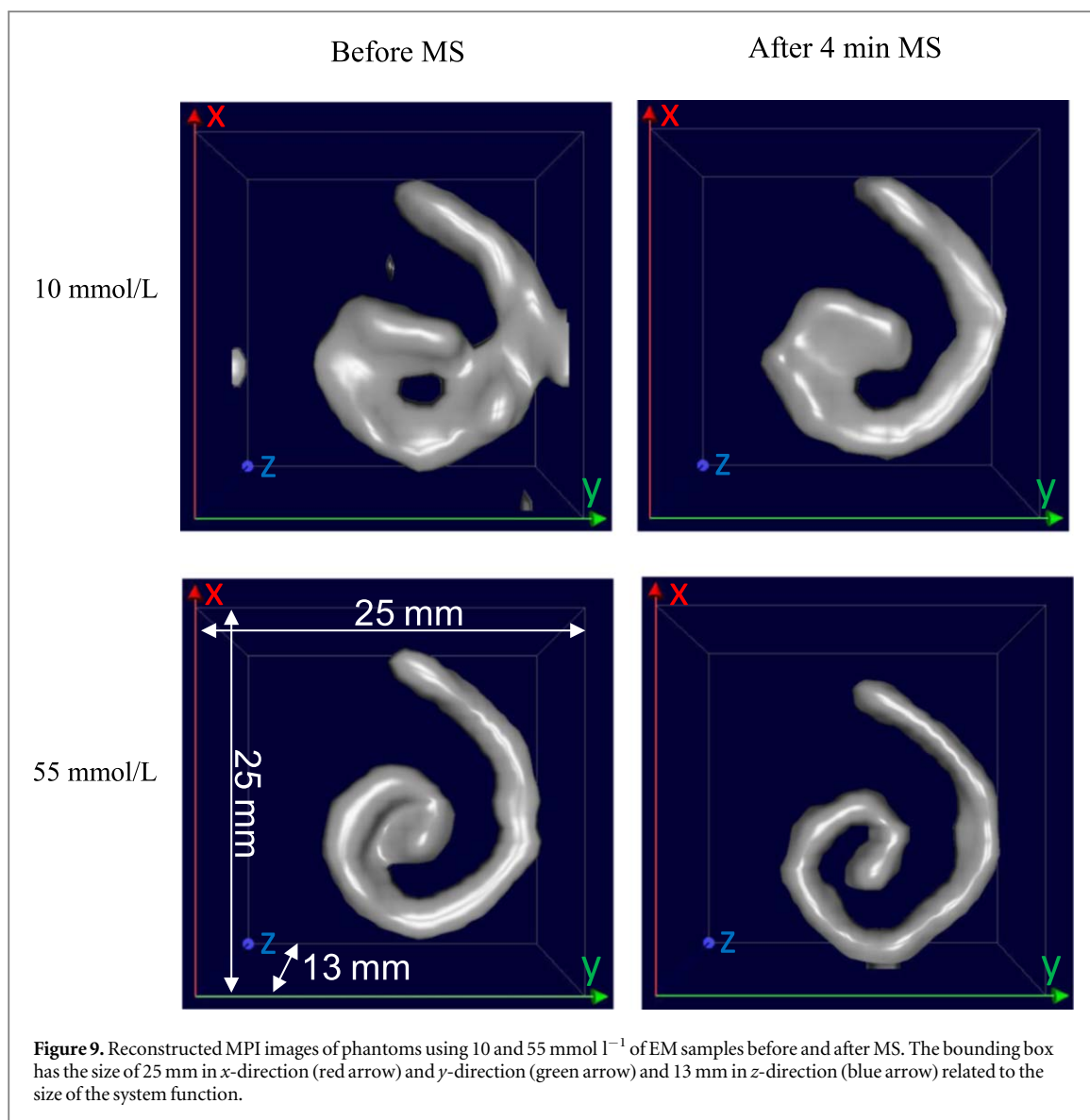
there is a clear frequency shift of the maxima of χ' and χ'' components in all samples, starting with an EM sample before MS and followed by a significant shift after 3 min, 50 min and 3 h of MS. Figure 4(b) shows that the χ'' peak shifts towards higher frequencies after 3 h of separation which indicates a reduction of the MNP size.

Table 1 shows the d_h and σ considerably reduced after 3 min of separation, while minor differences can be observed afterwards (50 min, 3 h).

The third harmonic amplitude normalized to the iron amount (A_3^*) and harmonic ratio A_5/A_3 of MPS signal versus separation time for EM10 sample have shown in figures 5(a), (b), respectively. Table 1 shows that the A_3^* and A_5/A_3 parameters improve about 35% and 11%, respectively, after up to 3 h of separation.

Furthermore, the magnetophoretical behavior of EM samples with different concentrations from 2 to 120 mmol l^{-1} for 24 h separation was recorded (figure 6(a)). The results show the primary opacity samples increase and separation time decrease by increasing the concentration of MNP up to 15 mmol l^{-1}, then for higher concentrations the primary opacity does not considerably change and the first step disappeared (figure 6(a)), that can be attributed to the opacity saturation for high concentrated sample. To verify this, we recorded the primary opacity of two colors of inks such as black and blue with increasing percentage of concentration (0.1–100, v/v). The results (figure 6(c)) show that opacity gets saturated for samples at high ink concentrations, confirming the saturated opacity for EM samples with high concentrations of MNP.

Figure 9. Reconstructed MPI images of phantoms using 10 and 55 mmol l^{-1} of EM samples before and after MS. The bounding box has the size of 25 mm in *x*-direction (red arrow) and *y*-direction (green arrow) and 13 mm in *z*-direction (blue arrow) related to the size of the system function.

Table 2. DLS and MPS measurements of all EM samples after 4 min of MS.

Samples	dh (DLS) (nm)	PDI (DLS) (nm)	A_3^* (Am^2 kg^{-1} (Fe))	A_5/A_3 (%)
EM2	75	0.19	8.38	24.21
EM4	71	0.17	8.60	24.20
EM8	59	0.15	8.72	24.41
EM15	57	0.14	9.21	24.77
EM30	56	0.14	10.19	25.21
EM60	51	0.12	10.38	25.57
EM120	47	0.11	10.59	26.60

The DLS measurements of the EM samples with different concentrations for the time point $t = 4$ min of MS were shown in figure 7(a). As mentioned before, we ascribe this first accumulation to be caused by agglomerated MNP occurring within the first 4 min of separation (figure 6(a)).

In figures 7(b), (c) it can be seen that both d_h and PDI of the samples significantly decrease with regard to their MNP concentration within the first 4 min of MS.

The A_3^* and A_5/A_3 parameters of each sample were determined 4 min after MS to evaluate samples as MPI tracers. The results show the improvement of both A_3^* and A_5/A_3 by increasing the concentration of MNP in suspension. Table 2 summarizes parameters extracted from DLS and MPS measurements for EM samples extracted 4 min after MS.

Table 3. Selected frequency components for image reconstruction by the SNR $\geqslant 4$.

Usable frequency components	Before MS	After MS
10 mmol l^{-1}	337	424
55 mmol l^{-1}	998	1253

The image of the phantom filled with 200 μl of tracer is shown in figure 8 to compare with the reconstructed MPI images. The images of EM15 and EM120 samples after 4 min of separation with 10 and 55 mmol l^{-1} concentrations, respectively, and EM samples without applying separation diluted to the same concentration are shown in figure 9. For both concentrations a higher MPI image resolution was obtained compared to the respective sample before MS.

We observe this benefit of MS already during the image reconstructions by the number of usable frequency components selected by the SNR $\geqslant 4$ for both EM15 and EM120 samples. The MS improves the SNR of the recorded SFs and in this matter the number of usable frequency components for the image reconstruction is increased, see table 3. The image reconstruction results in better resolution and less artefacts by the increased SNR in the MPI signal. Applying the resolution analysis in (Kosch *et al* 2019) determined by the reconstructed gap between the neighboring channels, we achieve for 10 mmol l^{-1} before MS a resolution limit of 4.0 mm and after MS of about 2.5 mm and for higher concentration of 55 mmol l^{-1} a resolution of about 2.1 mm before MS and after MS of about 1.7 mm.

4. Discussion

Our results show that the magnetophoresis process for EM is reproducible and reversible and thus, makes the experiments more reliable. The advantage of the reversible process is the possibility of several measurement repetitions of the same sample leading to more trustworthy data. In addition, since the agglomeration/accumulation of MNPs is reversible, samples after MS can directly be applied for other applications or measurements, therefore not wasting any sample material.

The magnetophoresis curve of EM10 showed two distinct steps over a 14 h time period (figure 3(a)). Corresponding DLS results of samples taken at different time points of separation (t_0–t_3) strongly suggest the separation of magnetic entities of different sizes. First, larger individual MNP or MNP agglomerates are removed. Due to their larger magnetic moment they are moved by stronger attractive forces to the Eppendorf wall. Furthermore, these larger MNP could tend to form fast moving aggregates (e.g. chains), which result in the observed smaller d_h and PDI after t_1 (3 min after separation), as well. After accumulation of those MNP at the wall, remaining smaller MNP, are more slowly moved towards the wall leading to the second accumulation. Furthermore, the corresponding ACS results of these samples demonstrate that the d_h and σ are significantly reduced after t_1 suggesting the elimination of agglomerated MNP from the suspension during 3 min of MS for this sample. These results confirm the DLS results, however, the d_h measured by DLS is larger compared to the ACS result. Note that the DLS scattering intensity depends on the 6th power of the particle size leading to an over-interpretation of the average size, especially in heterogeneous samples (see the supporting information is available online at stacks.iop.org/PMB/66/015002/mmedia for DLS curves as number average diameters at different time points of separation). For this EM sample, both the A_3^* and A_5/A_3 MPS parameters increase with separation time that can be attributed to the removal of agglomerated MNP from the suspension and narrowing the magnetic moment distribution, resulting in improved the performance of this sample in biomedical applications such as MPI.

All MNP based biomedical applications like MPI, MRI, drug delivery and hyperthermia, demand to apply MNP of specific size, size distribution and magnetic behavior to obtain optimum performance. Therefore, time-controlled separation of MNP can be used to isolate the suitable size distribution and efficient magnetic properties of MNP (see the results for EM10 sample in table 1) for a desired biomedical application. Recent studies have reported a sequential centrifugation protocol to control the size and size distribution of MNP for application in MPI, MRI and hyperthermia (Dadfar *et al* 2020). By this, the improved imaging and hyperthermia performance after a sequential centrifugation was demonstrated. However, sequential centrifugation is a time-consuming and complex process to separate the MNP. By using the MS system, these limitations are overcome making it more rapid, facile, controllable and reproducible.

Furthermore, the magnetophoresis results of EM samples with different concentrations showed that the separation time decreases with increasing the MNP concentration from 2 to 15 mmol l^{-1} (figure 6(a)). In the magnetophoresis curve of the sample with the lowest concentration, EM2, no significant accumulation was observed that can be attributed to the low number of MNP in suspension which results in lower interactions of MNP with neighbors and no chains or aggregates are formed. Therefore, a slower separation process will occur

for this sample. This result is in a good agreement with the studies that were reported by De Las Cuevas *et al* (2008). They also showed that the separation time decreases by increasing the concentrations from 0.1 to 180 mmol l^{-1} (0.01–10 g l^{-1}) in a homogeneous 30 T m^{-1} gradient. However, in the present study, we used a magnetophoresis device with a 15 T m^{-1} gradient thus providing less magnetic forces on the MNP. Note, the magnetophoresis systems based on their size have different magnitude of gradient, for instance magnetophoresis systems that provide bigger sample container have a higher magnetic field gradient than 15 T m^{-1} in order to provide bigger magnetic forces, decreasing the separation time of MNP.

Moreover, the magnetophoresis results showed that by further increasing the MNP concentration ($>$30 mmol l^{-1}) the opacity gets saturated so that the first step for these samples (figure 6(a)) is no longer visible. In this case, the MNP concentrations are too high so that the photo diode is no longer capable to resolve concentration changes occurring during the removal of larger entities. The resulting disappearance of the first MNP accumulation at highly concentrated samples is a limitation of the magnetophoresis system that we used.

The DLS and MPS results of EM samples showed that d_h and PDI decreases and the A_3^* and A_5/A_3 parameters increase with increasing MNP concentration from 2 to 120 mmol l^{-1} within the time point t = 4 min of MS. Increasing the concentrations of MNP in suspension leads to an increase of the interactions between MNP and making longer chains and aggregations favorable. Therefore, agglomerated MNP which possess larger size and magnetic moment move faster towards the Eppendorf wall (De Las Cuevas *et al* 2008), whereby particles with smaller d_h and PDI remain in the Eppendorf center used for detection by the photo diode. Therefore, based on the obtained results in table 2 it can be concluded that the separation process is more effective and quicker for samples with high concentrations, such as 120 mmol l^{-1}, and that these samples already after the short separation time of 4 min exhibit the lowest PDI and highest A_5/A_3 and thus, can be considered as most efficient MPI tracers compared to the other samples. As a result, the sample after 4 min separation showed a higher MPI image resolution compare to the non-separated one as displayed in figure 9. Therefore, by applying the magnetophoresis system for a short separation time only for a few minutes we can improve the magnetic properties of samples, resulting in improved MPI performance.

Based on all the aforementioned discussion and experimental data one of the possible future works with MS system is to study the aggregation behavior of MNP with different size, zeta potential and surface coating in different biological media, for instance blood plasma.

5. Conclusion

In this work we employed commercial IONP (EM) in aqueous phase for LGMS ($<$15 T m^{-1}) to improve their performance as MPI tracer. We demonstrated that the LGMS technique is capable of separating larger MNP entities from the suspension in a short period of time which allowed us to adjust the size distribution and magnetic properties of MNP via time-controlled MS. Finally, EM samples after LGMS showed higher image resolution in MPI compared to the sample in initial state. Therefore, it can be concluded that the LGMS method is an efficient, reproducible and fast method for MNP size selection and capable of adjusting the functional properties of MNP for biomedical applications.

Acknowldgments

ORCID iDs

Soudabeh Arsalani   https://orcid.org/0000-0002-1957-7956
Oswaldo Baffa   https://orcid.org/0000-0002-0622-2814

References

Ahrentorp F, Blomgren J, Jonasson C, Sarwe A, Sepehri S, Eriksson E, Kalaboukhov A, Jesorka A, Winkler D and Schneiderman J F 2017 Sensitive magnetic biodetection using magnetic multi-core nanoparticles and RCA coils *J. Magn. Magn. Mater.* **427** 14–8

Andreu J, Camacho J, Faraudo J, Benelmekki M, Rebollo C and Martínez L M 2011 Simple analytical model for the magnetophoretic separation of superparamagnetic dispersions in a uniform magnetic gradient *Phys. Rev.* E **84** 021402

Arami H, Khandhar A, Liggitt D and Krishnan K M 2015 *In vivo* delivery, pharmacokinetics, biodistribution and toxicity of iron oxide nanoparticles *Chem. Soc. Rev.* **44** 8576–607

Araujo J F, Arsalani S, Freire F L Jr, Mariotto G, Cremona M, Mendoza L A, Luz-Lima C, Zaman Q, Del Rosso T and Baffa O 2020 Novel scanning magnetic microscopy method for the characterization of magnetic nanoparticles *J. Magn. Magn. Mater.* **499** 166300

Arsalani S, Arsalani S, Hadadian Y, Sampaio D R, Baffa O, Pavan T Z and Carneiro A A O 2019a The effect of magnetization of natural rubber latex-coated magnetite nanoparticles on shear wave dispersion magneto-motive ultrasound *Phys. Med. Biol.* **64** 215019

Arsalani S, Guidelli E J, Araujo J F D F, Bruno A C and Baffa O 2018 Green synthesis and surface modification of iron oxide nanoparticles with enhanced magnetization using natural rubber latex *ACS Sustain. Chem. Eng.* **6** 13756–65

Arsalani S, Guidelli E J, Silveira M A, Salmon C E, Araujo J F, Bruno A C and Baffa O 2019b Magnetic Fe$_3$O$_4$ nanoparticles coated by natural rubber latex as MRI contrast agent *J. Magn. Magn. Mater.* **475** 458–64

Arsalani S, Oliveira J, Guidelli E J, Araujo J F, Wiekhorst F and Baffa O 2020 Synthesis of radioluminescent iron oxide nanoparticles functionalized by anthracene for biomedical applications *Colloids Surf.* A **602** 125105

Benelmekki M, Caparros C, Montras A, Gonçalves R, Lanceros-Mendez S and Martinez L M 2011 Horizontal low gradient magnetophoresis behaviour of iron oxide nanoclusters at the different steps of the synthesis route *J. Nanopart. Res.* **13** 3199–206

Benelmekki M, Martinez L M, Andreu J, Camacho J and Faraudo J 2012 Magnetophoresis of colloidal particles in a dispersion of superparamagnetic nanoparticles: theory and experiments *Soft Matter* **8** 6039–47

Biederer S, Knopp T, Sattel T, Lüdtke-Buzug K, Gleich B, Weizenecker J, Borgert J and Buzug T 2009 Magnetization response spectroscopy of superparamagnetic nanoparticles for magnetic particle imaging *J. Phys. D: Appl. Phys.* **42** 205007

Dadfar S M, Camozzi D, Darguzyte M, Roemhild K, Varvarà P, Metselaar J, Banala S, Straub M, Güvener N and Engelmann U 2020 Size-isolation of superparamagnetic iron oxide nanoparticles improves MRI, MPI and hyperthermia performance *J. Nanobiotechnol.* **18** 1–13

De Las Cuevas G, Faraudo J and Camacho J 2008 Low-gradient magnetophoresis through field-induced reversible aggregation *J. Phys. Chem.* C **112** 945–50

Du Y, Lai P T, Leung C H and Pong P W 2013 Design of superparamagnetic nanoparticles for magnetic particle imaging (MPI) *Int. J. Mol. Sci.* **14** 18682–710

Gutiérrez L, Moros M, Mazario E, de Bernardo S, de la Fuente J M, del Puerto Morales M and Salas G 2019 Aggregation effects on the magnetic properties of iron oxide colloids *Nanotechnology* **30** 112001

He J, Huang M, Wang D, Zhang Z and Li G 2014 Magnetic separation techniques in sample preparation for biological analysis: a review *J. Pharm. Biomed. Anal.* **101** 84–101

Kosch O, Paysen H, Wells J, Ptach F, Franke J, Wöckel L, Dutz S and Wiekhorst F 2019 Evaluation of a separate-receive coil by magnetic particle imaging of a solid phantom *J. Magn. Magn. Mater.* **471** 444–9

Latham A H, Freitas R S, Schiffer P and Williams M E 2005 Capillary magnetic field flow fractionation and analysis of magnetic nanoparticles *Anal. Chem.* **77** 5055–62

Leong S S, Ahmad Z, Camacho J, Faraudo J and Lim J 2017 Kinetics of low field gradient magnetophoresis in the presence of magnetically induced convection *J. Phys. Chem.* C **121** 5389–407

Leong S S, Ahmad Z, Low S C, Camacho J, Faraudo J and Lim J 2020 Unified view of magnetic nanoparticle separation under magnetophoresis *Langmuir* **36** 8033–55

Leong S S, Yeap S P and Lim J 2016 Working principle and application of magnetic separation for biomedical diagnostic at high-and low-field gradients *Interface Focus* **6** 20160048

Lim J, Lanni C, Evarts E R, Lanni F, Tilton R D and Majetich S A 2011 Magnetophoresis of nanoparticles *ACS Nano* **5** 217–26

Lim J, Yeap S P, Leow C H, Toh P Y and Low S C 2014 Magnetophoresis of iron oxide nanoparticles at low field gradient: the role of shape anisotropy *J. Colloid Interface Sci.* **421** 170–7

Löwa N, Knappe P, Wiekhorst F, Eberbeck D, Thünemann A F and Trahms L 2015a Hydrodynamic and magnetic fractionation of superparamagnetic nanoparticles for magnetic particle imaging *J. Magn. Magn. Mater.* **380** 266–70

Löwa N, Radon P, Gutkelch D, August R and Wiekhorst F 2015b Hyphenation of field-flow fractionation and magnetic particle spectroscopy *Chromatography* **2** 655–68

Ludwig F, Balceris C, Jonasson C and Johansson C 2017 Analysis of ac susceptibility spectra for the characterization of magnetic nanoparticles *IEEE Trans. Magn.* **53** 1–4

Mohammed L, Gomaa H G, Ragab D and Zhu J 2017 Magnetic nanoparticles for environmental and biomedical applications: a review *Particuology* **30** 1–14

Pacakova B, Kubickova S, Reznickova A, Niznansky D and Vejpravova J 2017 Spinel ferrite nanoparticles: correlation of structure and magnetism *Magnetic Spinels—Synthesis Properties and Applications* (London: IntechOpen Ltd.) pp 4–6

Petosa A R, Jaisi D P, Quevedo I R, Elimelech M and Tufenkji N 2010 Aggregation and deposition of engineered nanomaterials in aquatic environments: role of physicochemical interactions *Environ. Sci. Technol.* **44** 6532–49

Rahmer J, Weizenecker J, Gleich B and Borgert J 2009 Signal encoding in magnetic particle imaging: properties of the system function *BMC Med. Imaging* **9** 4

Rahmer J, Weizenecker J, Gleich B and Borgert J 2012 Analysis of a 3D system function measured for magnetic particle imaging *IEEE Trans. Med. Imaging* **31** 1289–99

Stephens J R, Beveridge J S and Williams M E 2012 Analytical methods for separating and isolating magnetic nanoparticles *Phys. Chem. Chem. Phys.* **14** 3280–9

Umar A and Atabo S 2019 A review of imaging techniques in scientific research/clinical diagnosis *MOJ Anat. Physiol.* **6** 175–83

Wu L, Zhang Y, Steinberg G, Qu H, Huang S, Cheng M, Bliss T, Du F, Rao J and Song G 2019 A review of magnetic particle imaging and perspectives on neuroimaging *Am. J. Neuroradiol.* **40** 206–12

Yavuz C T, Mayo J, William W Y, Prakash A, Falkner J C, Yean S, Cong L, Shipley H J, Kan A and Tomson M 2006 Low-field magnetic separation of monodisperse Fe$_3$O$_4$ nanocrystals *Science* **314** 964–7

Yeap S P, Lim J, Ooi B S and Ahmad A L 2017 Agglomeration, colloidal stability, and magnetic separation of magnetic nanoparticles: collective influences on environmental engineering applications *J. Nanopart. Res.* **19** 368

Yoshida T, Sasayama T and Enpuku K 2017 Effect of core size distribution of immobilized magnetic nanoparticles on harmonic magnetization *Int. J. Magn. Part. Imaging* **3** 1703002

Ziemian S, Löwa N, Kosch O, Bajj D, Wiekhorst F and Schütz G 2018 Optimization of iron oxide tracer synthesis for magnetic particle imaging *Nanomaterials* **8** 180